Modification of braid-reinforced cellulose acetate hollow fiber membrane by doping graphene oxide

Zuwei Fan[a,b], Changfa Xiao[a,b,*], Qinglin Huang[b], Binjie Tang[b]

[a]State Key Laboratory of Separation Membranes and Membrane Processes, Tianjin Polytechnic University, Tianjin 300387, China, No. 399 Binshui West Street, Xiqing District, Tianjin 300387, Tel. +86 22 83955299, email: xiaochangfa@163.com (C. Xiao)
[b]Research Institute, Beijing E&E Technologies Group Corporation Limited, Beijing 100044, China

ABSTRACT

To improve the permeability, antifouling and mechanical performance of cellulose acetate (CA) hollow fiber membrane is the objective of this study. Braid-reinforced method, where a simple coating process is implemented with high-strength hollow tubular braid as the reinforcement, is adopted to prepare the reinforced CA hollow fiber membrane; and graphene oxides (GOs) with various sheet size and additive content are incorporated into the separation layer to optimize the permeability and antifouling performance of the membrane. Scanning electron microscopy (SEM) images show that the prepared membranes have a favorable interfacial bonding state between the separation layer and the braid; the more and longer finger-like macro-void and thinner skin layer appear in the separation layer after GOs modification. The pure water flux of membrane increases from 129.8 L/m²h to 158.1 L/m²h by introducing 1 wt% GO (with sheet size of 30–50 μm). Besides, the GOs modification brings about increased protein solution permeate flux and flux recovery during the protein solution filtration. The tensile strength (about 30 MPa) of the braid-reinforced membranes mainly depends on the braid, which is much higher than the conventional solution spinning hollow fiber membrane. Meanwhile, there is a decent boost in the bursting strength of the membrane by GOs modification.

Keywords: Braid-reinforced; Cellulose acetate; Graphene oxide; Hollow fiber membrane; Permeability; Strength

1. Introduction

Cellulose acetate (CA), the most important derivate of natural cellulose, has played a significant role in membrane separation because of its good film forming performance [1,2] and relatively low cost [3]. Desalination [4] and hemodialysis [5,6] are the established fields where CA membranes have been applied. Most CA hollow fiber membranes which are composed of skin layer and support layer are usually prepared through the immersion-precipitation method [5], where the poor mechanical property limits their application in engineering practice, especially in the membrane bioreactor (MBR). The hollow fiber membrane used in the submerged MBR is easy to be damaged and broken by the disturbance of the aerated airflow or high-pressure water washing process [7]. Therefore, in the use of such water treatment, the filtration membrane is required not only for its superior separation and permeation performance but also for its higher mechanical property than hitherto [8].

Some studies have been carried out to improve the mechanical properties of the hollow fiber membranes. Polyethylene terephthalate (PET) threads-reinforced polyvinylidene fluoride (PVDF) hollow fiber membranes were prepared by Liu et al. [9] and the tensile/rupture strength of the reinforced membranes were significantly improved to 10 MPa. But it is so demanding on technology to introduce

---

*Corresponding author.

PET threads into the membrane wall. A simpler and more effective method to prepare reinforced hollow fiber membrane had been proposed, in which a simple coating process is implemented with high-strength hollow tubular braid as the reinforcement [10]. However, such a hollow fiber membrane has a problem that the porous membrane is easy to peel off from the braid because the porous membrane and reinforced fiber are thermodynamically incompatible system [7]. The requirement of the interfacial bonding strength between the porous membrane and the reinforced fiber is higher than the tensile strength because of the techniques of aeration and antiwash in the filtration process.

Recently, graphene derivates have become ideal candidates for polymer reinforcement on account of their unique architecture and superior performance. Correspondingly, it can be incorporated into filtration membranes to optimize targeted properties, such as high water permeability, high solute rejection and better antifouling performance, by the solution-blending method [11–13]. Graphene oxide (GO) with oxygen-containing groups attached on its edge and basal plane is a highly dispersible derivate of graphene [14], and possesses remarkable chemical, mechanical and physical properties, such as extremely high specific surface area, superior mechanical strength, excellent wettability and a unique graphitized plane structure [15], which are important factors in enhancing the membrane properties when it is used in the mixed-matrix membranes. Several authors have investigated the influence of two-dimensional GO on permeation and antifouling performance of ultrafiltration membranes [11–13]. However, the study of GO in the performance modification of composite CA membrane has not been reported. In addition, the effect of the size of the GO nanosheet on the microstructure and performance of synthetic membrane has not been investigated in speciality.

To improve the mechanical performance of CA hollow fiber membrane, braid-reinforced method by coating process is adopted in this study. To overcome the above-mentioned thermodynamically incompatibility and enhance the interfacial bonding state between the separation layer and the reinforced braid, CA filament was partially incorporated into the polyacrylonitrile (PAN) braid as homogeneous-reinforced fiber. This method has been proposed in our previous work [16,17]. So, the problem of mechanical performance was resolved effectively and the preparation process was simple. Then graphene oxides (GOs) with various sheet size and additive content were incorporated into the separation layer by the solution-blending method to optimize the permeability and antifouling performance of the membrane, due to their unique structure and superior performance. The effects of the GO sheet size and the GO/CA ratio in coating solutions on the membrane structure, filtration and mechanical properties would be studied.

2. Experimental

2.1. Materials

Cellulose acetate (CA, Mw = 60,000) was purchased from Wuxi Chemical Industry Research & Design Institute Co., Ltd. N,N-dimethylacetimide (DMAc, 99.5%) and poly (ethylene glycol) (PEG, Mw = 600) were obtained from Tianjin Kermel Chemical Reagent Co., Ltd. Bovine serum albu-

min (BSA, Mw = 68,000) was bought from Beijing Solarbio Science & Technology Co., Ltd. Cellulose acetate filament yarn (CA fiber, 150D/30F) was provided by SVACO (Hong Kong) Ltd. Polyacrylonitrile filament yarn (PAN fiber, 150D/60F) was supplied by Changshu Xiangying Special Fiber Co., Ltd. Single-layer graphene oxides (GO-a, with sheet diameter of 0.5–5 µm; GO-b, with sheet diameter of 30–50 µm) were produced through improved Hummers' method [18] by Hengqiu Graphene Technology (Suzhou) Co., Ltd.

2.2. Membrane fabrication

All the membranes were prepared by the concentric circles coating and dry-wet spinning process. Before this process, three bundles of filament tows (consisted of a bundle of PAN filament tow and two bundles of CA filament tows) were combined into one filament tow by the doubling machine, and then the hollow tubular braids were prepared by the two-dimensional braiding machine using the combined tows. Then GO-a or GO-b (0, 0.5, 1 and 1.5 wt% based on the weight of CA) was first imported into DMAc solvent (70 g), and then the solutions were sonicated for 120 min (40 kHz) before addition of CA (15 g) and PEG (15 g). The dope solutions were then mechanically stirred at 70°C for at least 3 h. The braid-reinforced hollow fiber membranes were fabricated through the concentric circles coating setup showed in Fig. 1. In this process, the hollow tubular braids went through the glass coater, and the coating solution after fully degassing was added into the glass coater. Thus the braids were coated with the CA solutions and guided through a water coagulation bath (15°C) under the drawing of the wire guide roller, where the braid-reinforced CA hollow fiber membranes were formed. The air-gap distance and take-up speed were set at 20 cm and 120 cm/min, respectively. The resultant membranes were stored in water for at least 24 h to remove the residual solvents and wash out the water-soluble additive. In order to identify these membranes easily, they were denoted as CA, CA/GO-a and CA/GO-b, respectively.
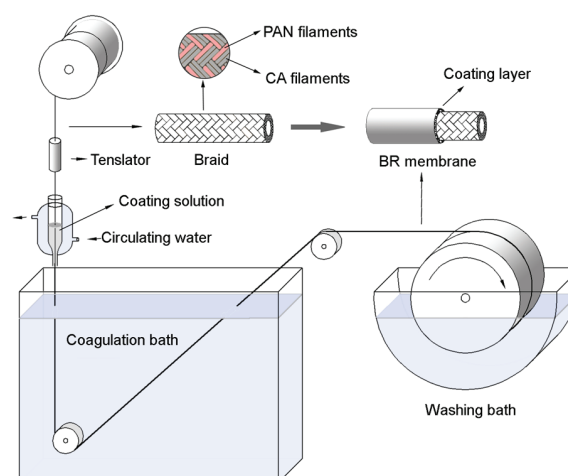

Fig. 1. Schematic diagram of the spinning apparatus.

2.3. GO characterization

The morphology of the GO was observed using transmission electron microscope (TEM, H-7650, HITACHI, Japan) operated at 120 kV. The surface morphology and sheet thickness of GO was examined using atomic force microscope (AFM, 5500 AFM/SPM, Agilent, USA). The GO was dispersed by sonication in a mixture of pure water, and then dried and the AFM tested under the tapping mode. Fourier-transform infrared spectrometer (FTIR, TENSOR37, BRUKER, Germany) was used to identify functional groups on the surface of the GOs.

2.4. Membranes characterization

To characterize the chemical property of the membranes, the separation layer was peeled off from the braid, and the FTIR measurements were carried out. The morphologies of the membranes were observed using scanning electron microscope (SEM, Quanta 200, FEI, Netherland). The water contained in the samples was substituted by ethyl alcohol, t-butanol/ethyl alcohol (1/1) and t-butanol for 12 h successively. Then the samples were freeze dried for 24 h, followed to be cut off by a razor blade. Thereafter, they were sputtered with gold and recorded through SEM.

The mean pore size of the each membrane was determined by using automatic mercury porosimeter (AutoPore IV-9500, Tektronix, USA). The hydrophilicity of membrane surface was characterized by water contact angle that was measured using a contact angle goniometer (DSA-100, KRÜSS, German). Static water angles contact were taken 10 s after the contacting of the drop with the surface.

2.5. permeation performance measurements

The pure water flux of the membranes was determined by a cross-flow batch (Fig. 2). The pressure difference across the membrane was 0.1 MPa under the condition of outside feeding.

The protein solution flux of the membranes was measured with 1000 mg/L BSA aqueous solution at 0.1 MPa. The BSA rejection was calculated from the BSA concentration in feed solution and permeate solution. The concentrat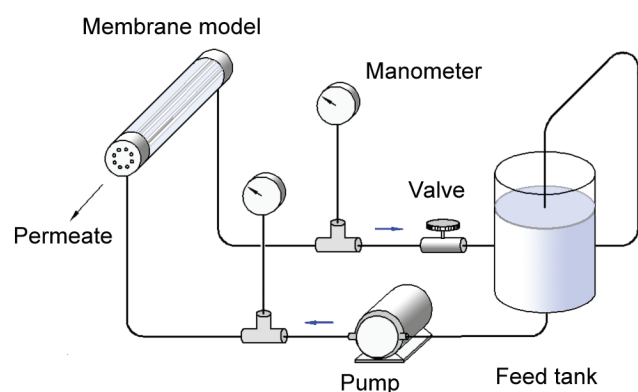ion of feed solution and permeate solution were determined by ultraviolet (UV) spectroscopy at wavelength of 280 nm, using a spectrophotometer (TU-1810, Purkinje General, China).

After BSA solution filtration for 60 min, the membranes were cross-flow cleaned with pure water for 10 min to recover their permeability. The flux recovery rate was calculated as the ratio of the pure water flux after cleaning to the pristine pure water flux.

2. 6. Mechanical property tests

The tensile properties of the hollow fiber membranes were tested at room temperature through electromechanical testing machine (JBDL-200N, Yangzhou Jingbo, China). The gripping range and tensile rate were 100 mm and 100 mm/min, respectively.

The interfacial shear strength between the coating layer and the braid was determined through pull-out test (Fig. 3a). The hollow fiber membrane was partially embedded in an epoxy resin, and only the coating layer with length of 1 cm contacted with the epoxy resin. The pull-out force of the braid from the coating layer/epoxy resin was measured through electromechanical testing machine and the pull-out strength was calculated using Eq. (1):

$$P = \frac{F}{\pi dl} \tag{1}$$

where P was the pull-out strength (Pa), F was the pull-out force (N), d was the diameter of the braid (m), and l was the length of the embedding membrane (m).

The bursting strength of the membranes was measured by using an apparatus with nitrogen cylinders, pressure gauge and gas flowmeter as shown in Fig. 3b.

3. Results and discussion

3.1. Characterization of GOs

Several characterization techniques (TEM, AFM and FTIR) were used to understand the unique physicochemical properties of GO nanosheets. The GOs prepared by the improved Hummers method have a yellowish/light brown color, indicating that the carbon lattice structure is distorted by the added oxygenated functional groups, since

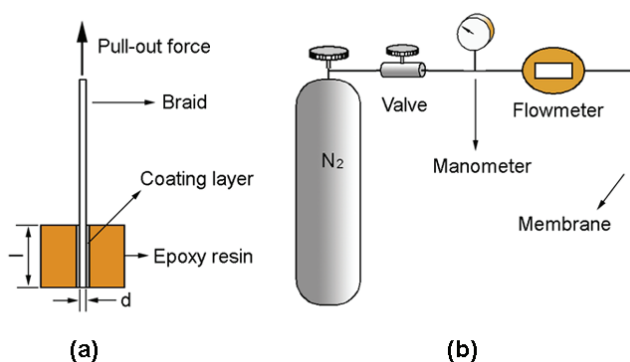Fig. 2. Schematic diagram of cross-flow filtration apparatus. [17]

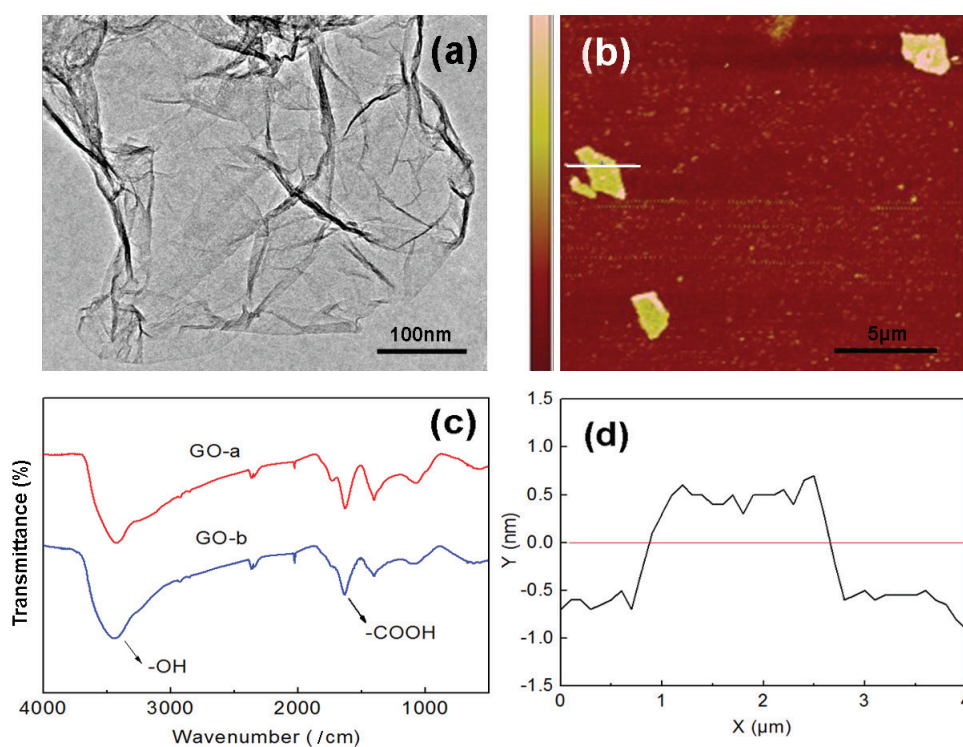Fig. 3. Schematic diagram of (a) pull-out test and (b) bursting test.

Fig. 4. Characterization of GO nanosheets. (a) TEM image, (b) AFM image, (c) FTIR spectra, (d) AFM height profile of GO.

pure graphene or graphite is black. Fig. 4a shows that the GO sheet is ultrathin and transparent, which indicates that the GO sheet have obviously high specific surface area. It is seen from the AFM image (Fig. 4b) that the lateral size of the GO nanosheet is 2 μm or so. The height profile (Fig. 4d) obtained by analyzing the AFM image demonstrates that the thickness of GO nanosheet is within a range of 1.0–1.5 nm, indicating the GO nanosheet contains either single or double layers of carbon lattice. In addition, the morphology of the other GO nanosheet (GO-b) was difficult to be observed by TEM and AFM, because of the larger size and pleated sheet.

FTIR is a powerful tool of investigating functional groups of the GOs. In Fig. 4c, the peaks emerging at 1680/cm and 3300–3600/cm correspond to carboxyl group and hydroxyl group, respectively. The hydrophilic properties of these oxygen-containing functional groups on the surface of the two kinds of GOs will be beneficial in evidencing the improvement of the dispersibility of GOs in aqueous solution and the membrane hydrophilicity.

3.2. Characterization of membranes

The FTIR spectra of the membrane separation layer are shown in Fig. 5. The neat CA membrane shows a band at 1742/cm, which is attributed to the stretching vibration of C=O. The band at 1230/cm in fingerprint region corresponds to the stretching modes of C–O single bond in acetates. Besides, there is no obvious absorption peak of O–H bond. These demonstrate that there are plenty of acetyl groups and few hydroxyl groups in the CA membrane. Compared with the spectrum of neat CA membrane, there
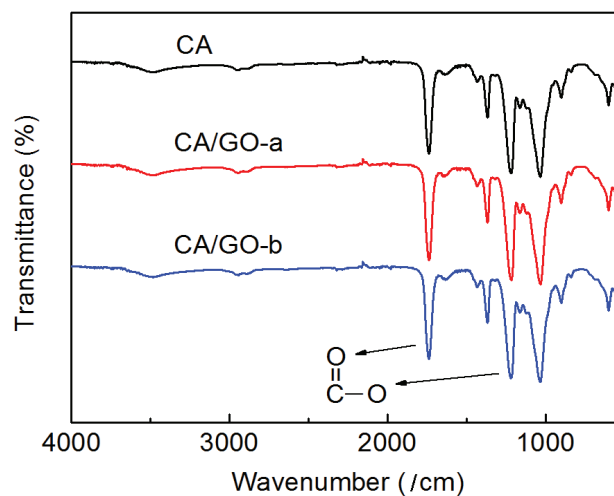

Fig. 5. FTIR spectra of the neat CA and 1 wt% GO modified CA membranes

is no obvious change in the GO modified CA membranes, which results from the low GO/CA ratio (1 wt%). The main effect of the modification of GOs is to change the structure of the membrane, which can be seen from the SEM photos.

In order to investigate the effect of GO modification on the microstructure of the membranes, SEM micrographs of braid-reinforced CA membrane and GO modified membranes have been obtained. As depicted in Fig. 6 (series 1), there is no obvious difference in the dense outer surface of the membranes. Fig. 6 (series 2 and 3) shows the cross-sec-
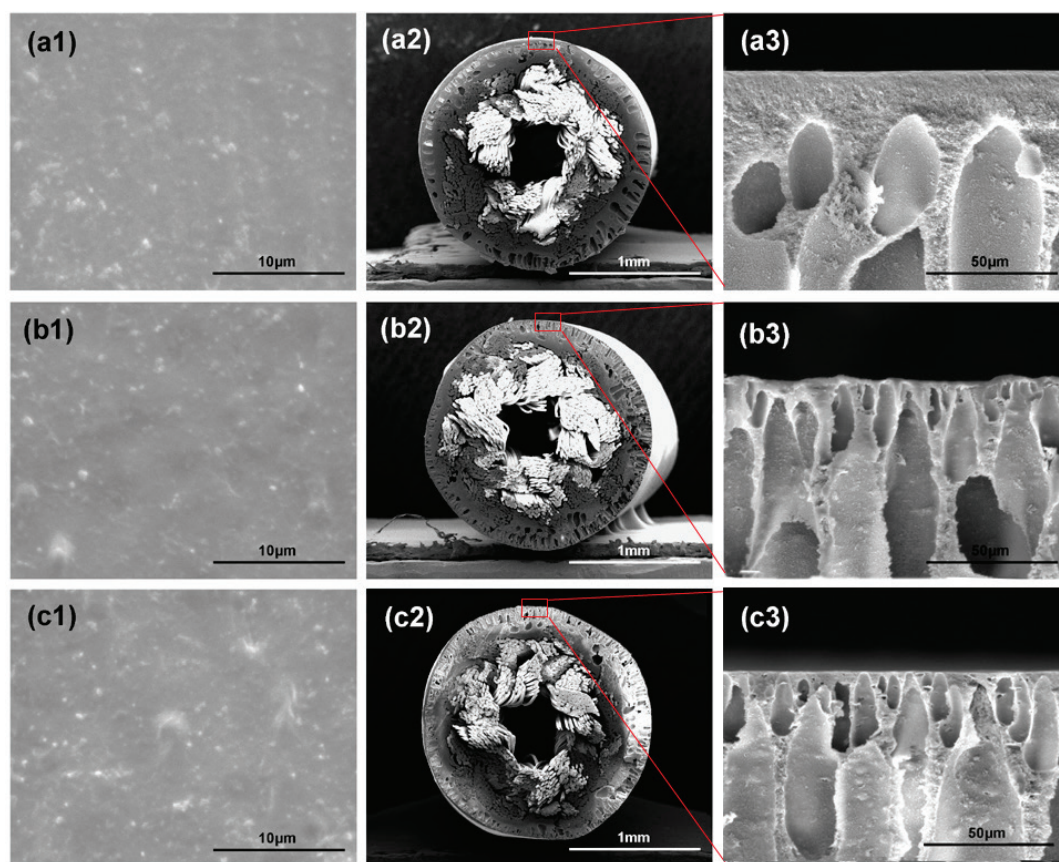
Fig. 6. SEM morphology of braid-reinforced hollow fiber membranes. (a) CA, (b) CA/GO-a (1 wt%), (c) CA/GO-b (1 wt%); (1) Outer surface, (2) Whole cross-section, (3) Enlarged separation layer.

tion and enlarged separation layer morphology views of the membranes. Obviously, a microporous coating layer is formed at the outer surface of the hollow tubular braid through the concentric circles coating method with the dope solution. There is favorable interfacial bonding between the separation layer and the braid due to the infiltration of the dope solution and the partial dissolution of CA fiber in the braid. The separation layer of all the membranes presents asymmetric structure with a selective thin upper skin on porous sub-layer with finger-like structure. This structure is mainly due to the mutual diffusivity of solvent (DMAc) and non-solvent (water). Compared with the neat CA membrane, the CA/GO-a and CA/GO-b membranes exhibit the more and longer finger-like macro-void and the longer finger-like macro-void results in the thinner skin layer. It can be explained by the affinity of GO with many types of hydrophilic groups, which increased mass transfer rate between solvent and non-solvent during phase inversion. Therefore, larger pore channels would form due to the rapid mass transfer [11]. The phenomena undoubtedly benefit the water permeability. Moreover, the used GO-a and GO-b have the similar chemical property, which can be seen from the FTIR spectra showed in Fig. 4c. So, little difference between the CA/GO-a and CA/GO-b membrane could be observed through the SEM images.

From Table 1, the mean pore sizes of the membranes are initially increased by incorporation of low amount of

GO and then, slightly reduced by more addition of GO. On one hand, the incorporation of GO increases the solution thermodynamic instability in the coagulation bath, which promotes a rapid phase demixing, resulting in large pore formation in low amount of the additives on the membrane surface [19]. On the other hand, the viscosity of blend solutions increases along with the content of GO. As a result, the increase of the viscosity typically delays the exchange of solvent and nonsolvent as well as suppresses the formation of large pore size. Besides, it could be seen that the GO modification has little impact on the surface hydrophilicity of the braid-reinforced CA membrane because of the low GO/CA ratio mentioned before.

3.3. Permeation performance

The addition of GO also have an impact on the permeation performance of the braid-reinforced CA membrane. Fig. 7a presents pure water flux and BSA rejection of the membranes. The pure water flux of the membranes are initially increased by incorporation of low amount of GO and then, reduced by more addition of the additives; the rejection of membranes decreases slightly with the addition of GO. Obviously, 1 wt% GO/CA membranes have the highest flux, and the CA/GO-b membranes present better permeability than the CA/GO-a membranes in

Table 1
Characterization of braid-reinforced hollow fiber membranes

| Membrane	GO/CA ratio (wt %)	Inner diameter (mm)	Outer diameter (mm)	Coating layer thickness (µm)	Skin layer thickness (µm)	Mean pore size (nm)	Contact angle (°)
CA	0	0.41 ± 0.07	1.83 ± 0.02	155 ± 33	21.7 ± 5.3	131	62.3 ± 4.1
CA/GO-a	0.5	0.42 ± 0.08	1.78 ± 0.01	162 ± 28	3.7 ± 0.9	151	62.7 ± 3.6
	1	0.37 ± 0.06	1.76 ± 0.03	174 ± 30	2.3 ± 0.7	214	63.8 ± 4.4
	1.5	0.40 ± 0.06	1.77 ± 0.02	159 ± 26	2.5 ± 0.7	204	61.4 ± 3.7
CA/GO-b	0.5	0.43 ± 0.07	1.79 ± 0.01	155 ± 31	3.2 ± 0.6	165	63.2 ± 3.1
	1	0.41 ± 0.06	1.82 ± 0.02	165 ± 34	2.7 ± 0.6	193	64.1 ± 4.3
	1.5	0.38 ± 0.07	1.78 ± 0.02	161 ± 29	3.6 ± 0.8	157	61.9 ± 4.0
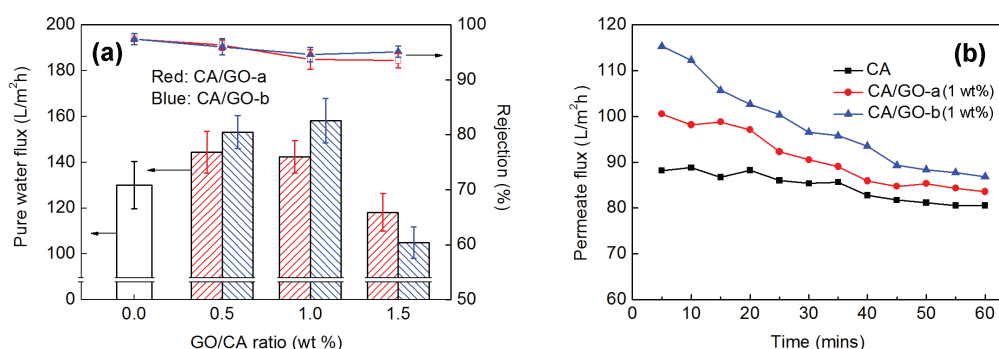
Fig. 7. Permeation performance of braid-reinforced hollow fiber membranes. (a) Pure water flux and BSA rejection; (b) Time-dependent BSA solution permeate flux.

low amount of GOs. The pure water flux of membrane increases from 129.8 L/m^2h to 158.1 L/m^2h by introducing 1 wt% GO-a. As shown in Fig. 8, the permeability of the membranes is affected by the water channels, which can be tuned by the GO content and GO structure. The thin skin layer in the separation layer plays a role of the main fluid flow resistance through the membrane. The membranes modified by GOs have the thinner skin layer (Table 1), which undoubtedly benefit the water permeability. This can be seen from the SEM photographs shown in Fig. 6 (series 3). On the other hand, some of the GO nanosheets existing in the CA matrix parallel to the membrane surface, which endow the water permeating with tortuous or zigzag channel [20] and undoubtedly generate membrane resistance. In addition, the length of the water channels in membrane is mainly determined by the GO content level and sheet size. GO-a has the better dispersion than GO-b because of the smaller sheet size, which could render the water channels longer and the pure water flux lower in GO/CA ratio of 0.5 and 1 wt%; As the GO loading increase, the membrane resistance caused by tortuous water channels per unit thickness increase (Table 2), which results in the reduced pure water flux in GO/CA ratio of 1.5 wt%. All things considered, the additive content of GO have more influence on the membrane permeability than the nanosheet size. As for the BSA rejection, the pore size of the membranes plays a crucial role, based on the sieving mechanism.
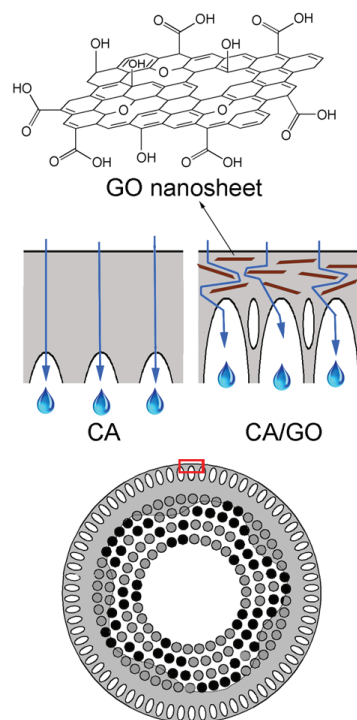

Fig. 8. Mechanism for water permeation through the skin layer.

Fig. 7b shows the variation with time of the flux in the permeation of protein solution under a fixed pressure (0.1 MPa). The initial protein solution fluxes of the GO modified CA membranes, especially the CA/GO-b membrane, are above that of the CA membrane; after filtration for 60 min, the steady fluxes of the GO modified CA membrane are still higher than the CA membrane. Besides, the CA membrane has a low flux decline rate of 8.6% during the protein solution filtration; while the flux decline degrees are 16.5% for the CA/GO-a (1 wt%) membrane and 24.7% for the CA/GO-b (1 wt%) membrane, which are higher than the neat membrane in spite of the higher protein solution flux (Table 3). The flux decline in the membrane filtration is attributed to two main sources: the concentration polarization and membrane fouling. Concentration polarization can be reduced by modifying the flow over the membrane (such as cross-flow velocity). The flux recovery rate is introduced to evaluate the fouling properties. From Table 3, the flux recovery rate values for the CA, CA/GO-a and CA/GO-b membranes are 91.2, 94.5 and 96.7%, respectively. The high flux recovery during the process of protein solution filtration indicates the anti-fouling properties of all the membranes are well. Thus, the incorporation of GO, especially GO-b, not only brings about increased permeate flux during the process of protein solution filtration, but also keeps the flux recovery rate at a high or higher value. These effectively reduce the frequency and strength of the washing process, which can indirectly improve the service life of the membranes.

Table 2
The resistance analysis of the membranes

Membrane	GO/CA ratio (wt %)	Membrane resistance ($\times 10^{12}$ m^{-1})	Membrane resistance / skin layer thickness ($\times 10^{17}$ m^{-2})
CA	0	2.77	1.28
CA/GO-a	0.5	2.49	6.73
	1	2.53	11.00
	1.5	3.05	12.21
CA/GO-b	0.5	2.35	7.34
	1	2.28	8.44
	1.5	3.43	9.53

Table 3
BSA solution filtration characterization of CA and 1 wt% GO modified CA membranes

Membrane	Initial protein solution flux (L/m²h)	Steady protein solution flux (L/m²h)	Flux decline rate (%)	Flux recovery rate (%)
CA	88.2	80.6	8.6	91.2
CA/GO-a	100.5	83.6	16.5	94.5
CA/GO-b	115.3	86.8	24.7	96.7

3.4. Mechanical performance

The high mechanical strength is the biggest advantage of braid-reinforced hollow fiber membrane. The stress-strain curve of the hollow tubular braid and the braid-reinforced hollow fiber membranes are shown in Fig. 9a. The initial modulus of the raw braid is below the braid-reinforced membranes, because of the transformation of the braid structure from loose condition to jamming condition at the initial stage of tension. While the coating layer of the braid-reinforced membranes which withstand the most forces restrains the transformation at the initial stage of tension. Besides, the elongation at break of the braid-reinforced CA membranes is lower than the braid. This results from that the dope solution which infiltrates into the braid reduces the fiber orientation at break. The tensile strength of the membranes is about 30 MPa, which is much higher than the conventional solution spinning hollow fiber membrane. It can also be seen that there is no obvious difference in the tensile curve of the membranes, and the tensile strength of all the membranes close to the braid, which indicates that the tensile strength of the braid-reinforced hollow fiber membranes mainly depend on the braid.

Unlike the tensile strength, the pull-out strength and bursting strength can reflect more the strength of the interface and coating layer, respectively. From Fig. 9b, the pull-
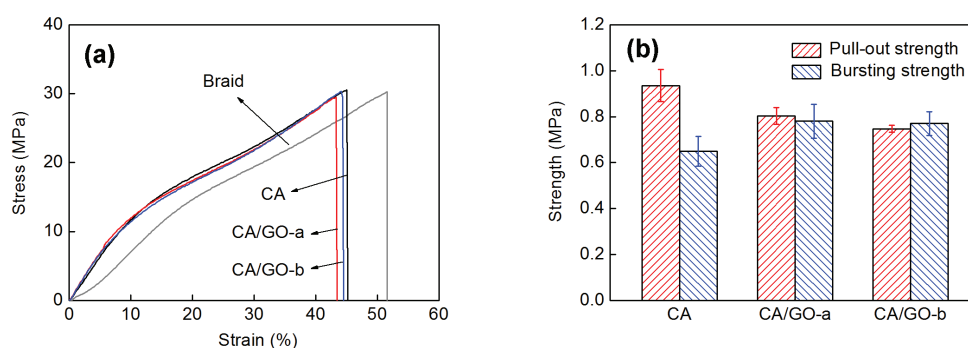

Fig. 9. Mechanical properties of neat CA and 1 wt% GO modified CA membranes. (a) Stress-strain curve; (b) Pull-out and bursting strength.

out strength of the GO modified CA membranes is slightly lower than the CA membrane, which could because that the higher viscosity of the CA/GO dope solutions leads to the lesser interface bonding strength due to the reduced infiltration and dissolution. Besides, the GO modified membranes acquire an increase in bursting strength compared with the CA membrane. This indicates that the porous coating layer of the modified membranes with GO are becoming stronger. The enhancement is attributed to that the brick-and-mortar architecture [21] and interfacial interaction can render effective load transfer. The GO nanosheet with extremely high specific surface area has a strong interaction with the CA matrix and the significantly improved adhesion at interfaces is obtained.

4. Conclusion

This study aims to improve the permeability, antifouling and mechanical performance of CA hollow fiber membrane. Braid-reinforced method, where a simple coating process is implemented with high-strength hollow tubular braid as the reinforcement, is adopted to prepare the reinforced CA hollow fiber membrane; and graphene oxides (GOs) with various sheet size and additive content are incorporated into the separation layer to optimize the permeability and antifouling performance of the membrane. SEM images showed that the braid-reinforced hollow fiber membranes have a favorable interfacial bonding state between the separation layer and the braid; the more and longer finger-like macro-void and thinner skin layer appeared in the separation layer by the addition of GOs. The maximum pure water flux (158.1 L/m²h) of GO modified CA membranes are obtained as the GO sheet size is 30–50 μm and the GO/CA ratio reaches to 1 wt%. The rejection of the membranes toward BSA decreases slightly because of the increased pore size after doping GOs. Introduction of 1 wt% GOs, especially with the larger sheet size of 30–50 μm, brings about increased protein solution permeate flux and flux recovery during the process of protein solution filtration, the increased flux recovery indicates that the anti-fouling properties of the braid-reinforced CA membranes are improved. The tensile strength (about 30 MPa) of the braid-reinforced membranes mainly depends on the braids, which is much higher than the conventional solution spinning hollow fiber membrane. Meanwhile, there is a decent boost in the bursting strength of the membrane by GOs modification.

In view of the conclusion discussed above, the braid-reinforced CA membrane possesses main advantage in mechanical performance which is barely affected by the composition of the coating solution. The membrane modified by GO hold a certain potential for improving the permeability and antifouling performance and need to be further exploited fully.

References

[1]   J. Amim Jr., P.M. Kosaka, D.F.S. Petri, Characteristics of thin cellulose ester films spin-coated from acetone and ethyl acetate solutions, Cellulose, 15 (2008) 527–535.
[2]   L.S. Blachechen, M.A. Souza, D.F.S. Petri, Effect of humidity and solvent vapor phase on cellulose esters films, Cellulose, 19 (2012) 443–457.
[3]   D.C. Brandt, G.F. Leitner, W.E. Leitner, Reverse osmosis membranes state of the art, In: Z. Amjad (Eds.), Reverse Osmosis Membrane Technology, Water Chemistry, and Industrial Applications, Van Nostrand Reinhold, New York, 1993. pp. 1–36.
[4]   O. Kutowy, S. Sourirajan, Cellulose acetate ultrafiltration membranes, J. Appl. Polym. Sci., 19 (1975) 1449–1460.
[5]   G. Dünweg, L. Steinfeld, W. Ansorge, Dialysis membrane made of cellulose acetate, US 5403485, 1995-04-04.
[6]   G. Sevillano, M. Rodriguez-Puyol, R. Martos, I. Duque, S. Lamas, M.L. Diez-marqués, J. Lucio, D. Rodríguez-Puyol, Cellulose acetate membrane improves some aspects of red blood cell function in hemodialysis patients, Nephrol. Dial. Transplant., 5 (1990) 497–499.
[7]   X.L. Zhang, C.F. Xiao, X.Y. Hu, Q.Q. Bai, Preparation and properties of homogeneous-reinforced polyvinylidene fluoride hollow fiber membrane, Appl. Surf. Sci., 264 (2013) 801–810.
[8]   X.L. Zhang, C.F. Xiao, X.Y. Hu, X.F. Li, R. Wang, Hydrophilic modification of high-strength polyvinylidene fluoride hollow fiber membrane, Polym. Eng. Sci., 54 (2014) 276–287.
[9]   J. Liu, P.L. Li, Y.D. Li, L.X. Xie, S.C. Wang, Z. Wang, Preparation of PET threads reinforced PVDF hollow fiber membrane, Desalination, 249 (2009) 453–457.
[10] M. Mailvaganam, L. Fabbricino, C.F.F. Rodrigues, A.R. Donnelly, Hollow fiber semipermeable membrane of tubular braid, US 5472607, 1995-12-05.
[11] Z.H. Wang, H.R. Yu, J.F. Xia, F.F. Zhang, F. Li, Y.Z. Xia, Y.H. Li, Novel GO-blended PVDF ultrafiltration membranes, Desalination, 299 (2012) 50–54.
[12] J. Lee, H.-R. Chae, Y.J. Won, K. Lee, C.-H. Lee, H.H. Lee, I.-C. Kim, J.-M. Lee, Graphene oxide nanoplatelets composite membrane with hydrophilic and antifouling antifouling properties for wastewater treatment, J. Membr. Sci., 448 (2013) 223–230.
[13] C.Q. Zhao, X.C. Xu, J. Chen, G.W. Wang, F.L. Yang, Highly effective antifouling performance of PVDF/graphene oxide composite membrane in membrane bioreactor (MBR) system, Desalination, 340 (2014) 59–66.
[14] D.R. Dreyer, S. Park, C.W. Bielawski, R.S. Ruoff, The chemistry of graphene oxide, Chem. Soc. Rev., 39 (2010) 228–240.
[15] H.B. Huang, Y.L. Ying, X.S. Peng, Graphene oxide nanosheet: an emerging star material for novel separation membranes, J. Mater. Chem. A., 2 (2014) 13772–13782.
[16] Z.W. Fan, C.F. Xiao, H.L. Liu, Q.L. Huang, Preparation and performance of homogeneous braid reinforced cellulose acetate hollow fiber membranes, Cellulose, 22 (2015) 695–707.
[17] Z.W. Fan, C.F. Xiao, H.L. Liu, Q.L. Huang, J. Zhao, Structure design and performance study on braid-reinforced cellulose acetate hollow fiber membranes, J. Membr. Sci., 486 (2015) 248–256.
[18] P.P. Wang, J. Ma, Z.H. Wang, F.M. Shi, Q.L. Liu, Enhanced separation performance of PVDF/PVP-g-MMT nanocomposite ultrafiltration membrane based on the NVP-grafted polymerization modification of montmorillonite (MMT), Langmuir, 28 (2012) 4776–4786.
[19] S. Liang, K. Xiao, Y.H. Mo, X. Huang, A novel ZnO nanoparticle blended polyvinylidene fluoride membrane for anti-irreversible fouling, J. Membr. Sci. 394 (2012) 184–192.
[20] K.T. Cao, Z.Y. Jiang, J. Zhao, C.H. Zhao, C.Y. Gao, F.S. Pan, B.Y. Wang, X.Z. Cao, J. Yang, Enhanced water permeation through sodium alginate membranes by incorporating grapheme oxides, J. Membr. Sci., 469 (2014) 272–283.
[21] Q. Zhao, Q.F. An, T. Liu, J.-T. Chen, F. Chen, K.-R. Lee, C.J. Gao, Bio-inspired polyelectrolyte complex/graphene oxide nanocomposite membranes with enhanced tensile strength and ultra-low gas permeability, Polym. Chem., 4 (2013) 4298–4302.